

Novel Lasers Based on Resonant Dark States

Sotiris Droulias,^{1,*} Aditya Jain,² Thomas Koschny,² and Costas M. Soukoulis^{1,2}

¹*Institute of Electronic Structure and Laser, FORTH, 71110 Heraklion, Crete, Greece*

²*Ames Laboratory and Department of Physics and Astronomy, Iowa State University, Ames, Iowa 50011, USA*

(Received 2 August 2016; published 17 February 2017)

The route to miniaturization of laser systems has so far led to the utilization of diverse materials and techniques for reaching the desired laser oscillation at small scales. Unfortunately, at some point all approaches encounter a trade-off between the system dimensions and the Q factor, especially when going subwavelength, mostly because the radiation damping is inherent to the oscillating mode and can thus not be controlled separately. Here, we propose a metamaterial laser system that overcomes this trade-off and offers radiation damping tunability, along with many other features, such as directionality, subwavelength integration, and simple layer-by-layer fabrication.

DOI: 10.1103/PhysRevLett.118.073901

As the laser dimensions are scaled down, less space is left for the gain material and, if low lasing thresholds are to be achieved (if lasing at all), light must interact with the gain material as much as possible. Simply put, the optical gain must effectively counteract the two dominant energy-loss channels, namely, the dissipative losses due to material absorption and the radiation damping due to the coupling of the oscillating mode to radiating waves.

All-dielectric systems [1–5] that sustain high Q modes can offer significantly low lasing thresholds, but their size is limited to the order of magnitude of the operating wavelength, by principle of operation. On the other hand, one can actually go subwavelength with the aid of surface plasmon-polariton modes, by incorporating some metal region into the system [6–14]. The necessary presence of metal nevertheless imposes large material losses and pushes the lasing threshold to high levels accordingly. More importantly, in all these implementations the radiation damping is closely connected with the type of the oscillating mode. If one desires to change the radiation damping at the given operating frequency, then the system must be redesigned to operate—if possible—with a different mode.

In this Letter, we propose a metamaterial laser system that resolves this predicament, by offering separate control of the energy storage and radiation mechanisms. The principle of operation is based on the excitation of a dark mode [15]; i.e., a mode of zero net electric or magnetic moment that does not consequently radiate. Ideally, in the total absence of any material loss, if energy is transferred into the system it will be stored in the dark mode and will stay there indefinitely. With the aid of a small nonresonant scatterer, though, the dark mode can be coupled to radiation modes at will. Then, the coupling of the dark mode to radiation waves can be simply controlled by the position, size, and material of the scatterer. In essence, the Q factor of the system is controlled at will and, most importantly,

independently of the resonance mechanism, which is responsible for the energy storage.

Our proposed laser consists of three basic parts: the gain material, the dark mode (which serves as the resonator), and the scatterer. In order to implement the resonator we choose a thin dielectric slab that supports a continuous dark bound state [red line in Fig. 1(b)] and then introduce silver scatterers of the same thickness d with a certain periodicity a . The purpose of the silver inclusions is to spatially quantize the modes of the dielectric slab, in order to tailor the desired mode distribution within the unit cell and to achieve a discrete set of resonant dark states [blue dots in Fig. 1(b)]. In essence, the dispersion of the composite metal-dielectric system becomes a quantized version of that of the dielectric slab, with periodicity π/a . Then, depending on the branch of the dispersion, an isolated mode with the desired operation frequency and spatial distribution can be chosen for operation. Here, we choose for simplicity the second of the quantized $TE_0^{(\text{even})}$ modes [red circle in Fig. 1(b)], which has an antisymmetric electric field profile with respect to the center of the slab [Fig. 1(a)] and is therefore dark (in general any higher-order nonradiative mode is suitable). Choosing the operating wavelength to be within typical telecommunication ranges of $1.5 \mu\text{m}$, the lattice constant of the unit cell is designed to be $a = 960 \text{ nm}$ and the width of silver $2w_m = 100 \text{ nm}$. The overall thickness of the metasheet is $d = 60 \text{ nm}$, which is thin enough to be subwavelength and can accommodate a gain material, such as a single quantum well [16,17]. The gain material is embedded in the dielectric of host permittivity $\epsilon_r = 12.1$ and the system is examined via self-consistent finite-difference time-domain calculations [18–22] (see Supplemental Material [23]).

First, with no scatterer present, we pump the system and monitor the electric field inside the slab, as well as the emitted power. Since the dark mode oscillates along the z axis, z -polarized waves are expected to be radiated. Indeed,

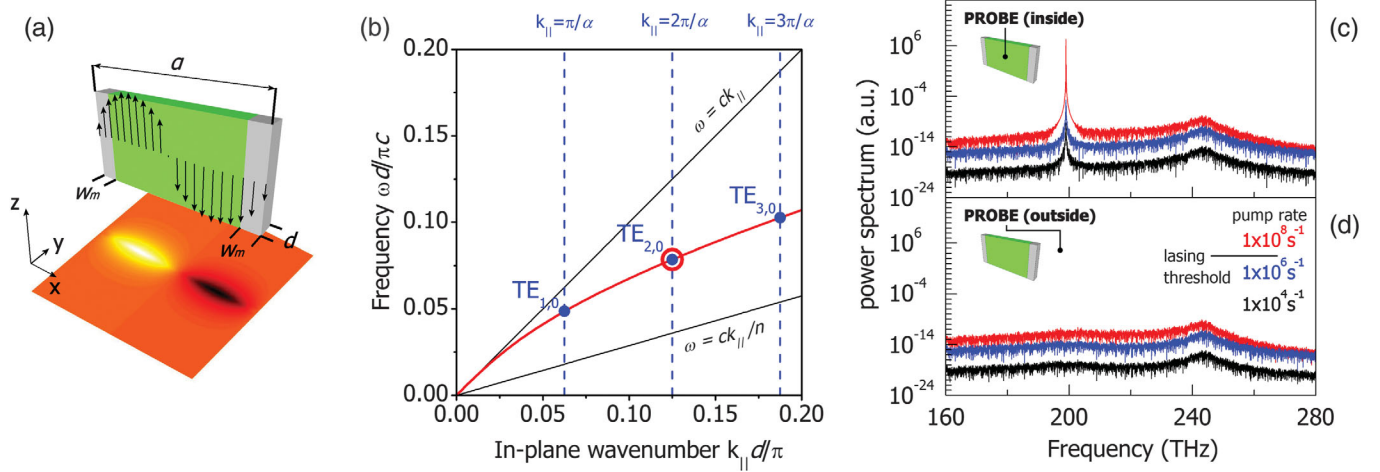


FIG. 1. The dark-mode laser principle of operation. (a) Perspective view of the unit cell, illustrating the spatial distribution of the dark mode, with which we work throughout this study [its operation point is marked in (b) with a red circle]. (b) Dispersion relation of the unpumped uniform dielectric slab of thickness d (red line) and quantized dispersion of the composite dielectric-metal system (blue dots). Power spectrum of the E_z field for several pump rates, when measured (c) inside and (d) away from the slab, without any scatterer present.

while for different pump rates the x , y components of the electric field behave as a pump-dependent noisy background, the picture is different for the E_z component. For low pump levels the power spectrum inside the slab has a peak at the dark mode frequency [Fig. 1(c)], which is not observed in the output spectrum [Fig. 1(d)], as the dark mode cannot couple to the free-space environment. Both spectra have nevertheless a feature around 240 THz, which is actually the signature of the $TE_{3,0}$ (bright) mode. After a pump rate of $R_p = 4.4 \times 10^6 \text{ s}^{-1}$ (corresponding to a pump intensity of $I_p = 17 \text{ mW/mm}^2$ [24]) we observe a transition to lasing. This is lasing into the dark mode which is therefore identified in the fields inside the slab only [Fig. 1(c)], and cannot be observed in the radiated power [Fig. 1(d)]. Hence, the output spectrum both below and above threshold looks similar without a distinct spectral peak [Fig. 1(d)]. The pumped power is stored in the dark mode. Now, in order to extract power to free space we couple it with radiating modes by placing the scatterer as shown in Fig. 2(a). Lasing can now be clearly identified in the measured emitted power as a transition from a low power spectrum into a sharp intense peak at the frequency of the dark mode [Fig. 2(a)]. At these levels, the pumped power is channeled into the dark mode to the degree that the neighboring spectrum receives less and less gain. This can be observed as a drop in the increase rate of the background spectrum.

The dielectric scatterer is placed on the surface with its center at distance $\delta x = 150 \text{ nm}$ ($\delta x/a \cong 0.16$) from the unit cell boundary [see inset of Fig. 2(a) and Fig. 3(a)]. It has the same permittivity as the slab and dimensions $w_{\text{scat}} = 60 \text{ nm}$ and $t_{\text{scat}} = 30 \text{ nm}$. At this position our calculations indicate that 20% of the supplied power is coupled outwards to radiation, while the rest 80% is dissipated on the silver. In fact, if the scatterer is removed,

then all supplied power is converted to Joule heating at the metallic scatterers, as confirmed by our simulations. The dark mode in fact lases, but does not couple to the environment and all power is channeled to dissipation. The same effect can be achieved with the scatterer present, if positioned exactly at the center of the unit cell ($\delta x = 480 \text{ nm}$ or $\delta x/a = 0.5$), as also confirmed by our simulations. In this case the scatterer does not break the mode's zy plane of symmetry, leaving no residual moment and thus maintaining the nonradiative character of the

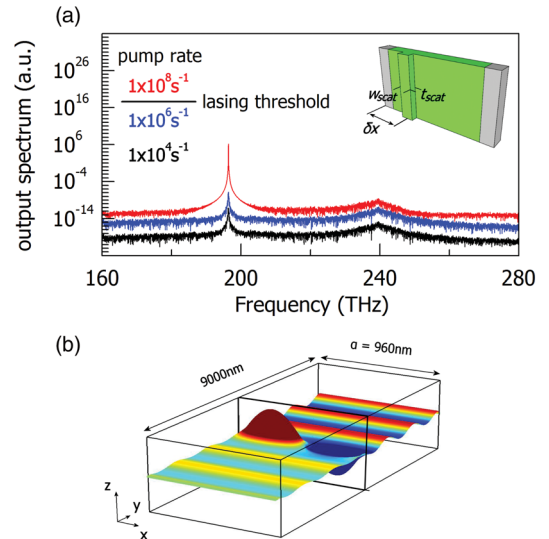


FIG. 2. Coupling of stored power to radiation. (a) Output power spectrum of the E_z field with scatterer placed at $\delta x = 150 \text{ nm}$ ($\delta x/a \cong 0.16$) (b) Snapshot during lasing. The unit cell position is marked with the lines framing the dark mode and its orientation is as shown in inset of (a); notice that most of the emitted power is directed to the side opposite to which the scatterer is located (calculated to be 90% of the total emitted power).

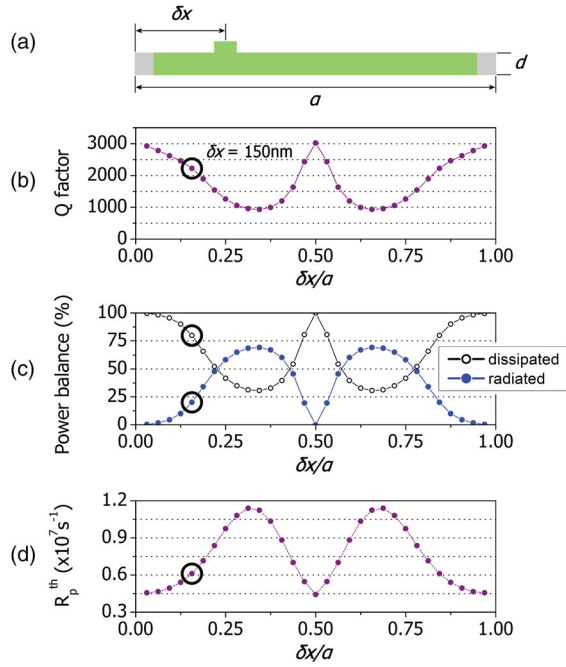


FIG. 3. Scanning the position of the scatterer (normalized with the unit cell width a). (a) Top view of unit cell; (b) Q factor; (c) radiated and dissipated power over supplied power; and (d) lasing threshold. The marked displacement $\delta x = 150$ nm ($\delta x/a \cong 0.16$) corresponds to the configuration for which lasing simulations are shown in Fig. 2, striking a balance between field enhancement (Q factor), outcoupling, and achievable directionality. Notice that at $\delta x/a = 0.5$ the Q factor is the maximum possible for this configuration (Q factor of the dark mode) and is limited only by the losses due to the metal. At this position the lasing threshold is the lowest possible and all lasing power, which cannot be radiated, is channeled to the metallic scatterers.

perturbed mode. At this position where the output power is minimized (middle of the unit cell), the lasing threshold acquires the minimum possible value for this specific design. The Q factor is maximized, with a maximum value limited only by the dissipative losses of the metal, which is calculated to be $Q = 3020$. As the scatterer is shifted along the unit cell, the coupling strength changes according to the shape of the dark mode; at positions where the fields are higher, the coupling is stronger and, hence, the radiation damping is stronger and the Q factor weaker [Fig. 3(b)]. Ideally, we would like to make radiation damping as small as possible, because weak coupling actually means that the ratio of the field strength inside to the field strength outside the dark mode is large. Since gain is proportional to $|E|^2$, this means that much more gain will be achieved and, hence, much more energy production inside the sample will be possible for the same pump energy. In turn, the radiated power will be effectively large. However, there is a trade-off, because there is an additional loss channel inside the structure. Consequently, if the radiation damping becomes smaller and smaller, first the Q factor—as well as the output—will increase as expected, but after some point the

internal losses will dominate and the Q factor will not further increase and diverge (as in the ideal case of zero intrinsic loss), but saturate. In effect, further reducing the coupling will reduce the output, as can be observed in Fig. 3(c). So, as the scatterer approaches the center position, the output power will decrease and the Q factor will saturate due to the intrinsic loss. The lasing threshold, which is also inherently related to the Q factor, is tuned accordingly [Fig. 3(d)]. Clearly, just by shifting the position of the scatterer we manage to control the emission and the radiation damping of the dark mode. Most importantly, these parameters can be tuned without intervening in the power storing mechanism, contrary to other spasinglike systems.

The subwavelength nature of the configuration makes it essentially a surface or radiating current sheet. If we put aside the detailed geometry for the moment and consider an infinite current sheet which radiates exactly as our system, then the emission of such a sheet can be controlled by an appropriate mixture of an electric \mathbf{j}_e and a magnetic \mathbf{j}_m current. The magnitude of the time-averaged Poynting vector along each side of the current sheet is expressed in this case as [25]

$$\langle S \rangle^\pm = \frac{1}{8\eta} (|\eta j_e|^2 + |j_m|^2 \pm 2|\eta j_e||j_m| \cos(\delta\phi)), \quad (1)$$

where $\delta\phi$ is the phase difference between \mathbf{j}_e and \mathbf{j}_m , η is the free-space impedance, and the sign \pm denotes the respective direction of emission along the y axis. Each one of the currents alone emits symmetrically to both sides of the sheet [set $j_e = 0$ or $j_m = 0$ in (1), for example], but with a balanced contribution the sheet can be made purely directional, i.e., emitting only to one side. The benefit is apparent: the sheet may emit purely on one direction without the need of a metal reflector, which will introduce additional loss. In order to implement this concept with the actual system, the lasing mode has to be coupled simultaneously to an electric and a magnetic moment; this can be achieved by introducing an additional weak scatterer on the opposite side of the slab. In essence, the dark mode will induce polarization currents I_1, I_2 on the two scatterers, which subsequently radiate. These individual currents can be interpreted as a weighted mixture of a symmetric $I_S \sim I_2 + I_1$ and an antisymmetric $I_A \sim I_2 - I_1$ current of the combined double-scatterer system, i.e., as a weighted mixture of an electric moment and a magnetic moment that radiate individually (Fig. 4). Depending on the phase and amplitude of each moment, their superposition can enhance or cancel radiation along a certain direction according to Eq. (1).

In practice, the two contributions can be tuned by coupling each scatterer with different parts of the dark mode. Hence, directionality is tuned simply by shifting the position of the scatterers. To demonstrate the concept we placed another identical scatterer on the opposite side of the slab, as illustrated in Fig. 5(d). In Fig. 5(a) the calculated directionality is shown and in Fig. 5(c) the quantities $|\eta j_e|$

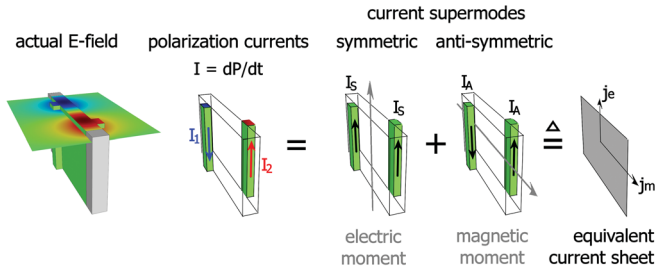


FIG. 4. Directionality explained via the equivalent current sheet model. The dark mode induces polarization currents I_1, I_2 on the two scatterers, which are effectively a weighted mixture of an electric moment and a magnetic moment that radiate individually. These moments are equivalently described by an infinite electromagnetic current sheet supporting an electric current \mathbf{j}_e and a magnetic current \mathbf{j}_m .

and $|j_m|$ are plotted for three characteristic cases, where emission is due to purely electric moment (A), purely magnetic moment (B), and due to equal electric and magnetic moment (C). The directionality for these cases is identified at the cross section shown in Fig. 5(b). Depending on the relative positions of the two scatterers, lasing can be achieved with any mixture of both moments. This is a significant advantage of our design, which effectively separates the resonant lasing state from the outcoupling and radiation, thus allowing us to tune them independently.

Our proposed system generalizes the concept of lasing into a dark surface state and is neither a Fabry-Perot laser (no propagating waves are coupled to radiation), nor a spaser (no stimulated emission of surface plasmons occurs and, hence, no surface plasmons are needed for operation). Compared to other plasmonic systems, it is also superior with respect to loss and can offer appreciably higher Q factors, as no real currents are involved, due to the dielectric implementation. Of course, due to the inclusion of metals, as a realistic and easy means for quantizing the fields, some losses are inevitably introduced. However, the losses can be designed to be low, not only by keeping the metal region as small as possible, but also because it will always overlap with a field minimum (node), by principle of operation. On the other hand metals have some advantages; they provide a convenient pathway for electrical contacting in the system (if gain is to be implemented by direct current injection) and allow for heat sinking. Because the metal wires are not pure zero field boundaries (there is a certain amount of cross talk between them), the individual unit cells will have a coherent dark mode. As a consequence, the lasing bound mode is an extended state across the surface and the radiated waves from the surface will be coherent. These coherent waves can be emitted, by principle of operation, perpendicular to the cavity and, hence, allow for the system to be deeply subwavelength along the emission direction, something not possible with typical Fabry-Perot lasers or photonic crystal lasers. This feature renders the system

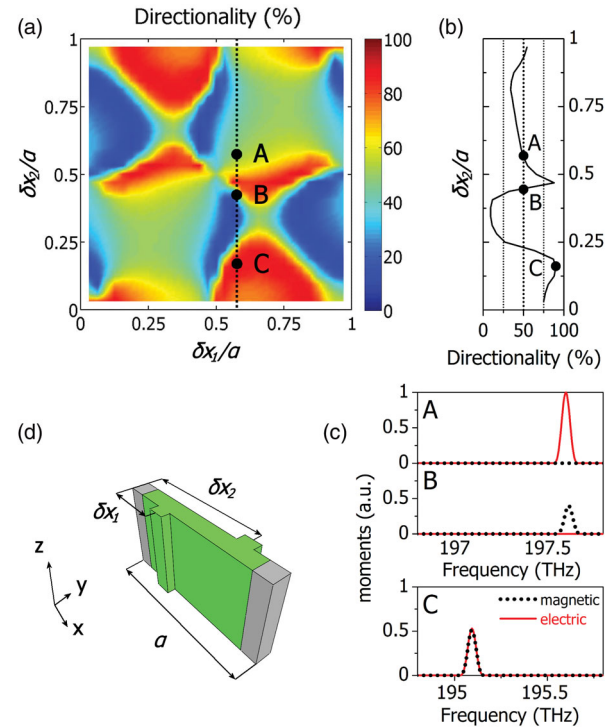


FIG. 5. Directionality vs scatterer displacement (normalized with the unit cell width a) in the double-scatterer configuration. (a) Directionality towards $y < 0$ (0–50 in scale) and $y > 0$ (50–100 in scale) as each scatterer is shifted along the unit cell. (b) Vertical cross section of Fig. 5(a) at $\delta x_1/a \cong 0.56$. (c) Electric (solid red line) and magnetic (dotted black line) moment (same scale) vs frequency, for three characteristic cases, also noted on panels (a) and (b) with the letters A, B, and C: A, for $\delta x_2/a \cong 0.56$, purely electric moment leading to a 50%–50% power split; B, for $\delta x_2/a \cong 0.44$, purely magnetic moment leading to a 50%–50% power split; C, for $\delta x_2/a \cong 0.16$, equal electric and magnetic moment leading to a 90%–10% power split. (d) Perspective view of the double-scatterer configuration.

essentially an emitting surface, which can be made as large as desired, offering highly collimated beams. The ultrathin vertically emitting geometry is ideal for subwavelength integration, giving promise for ultrasmall coherent light sources. Spatial arrangement of the scatterers may also offer tuning of the angular directionality, just as in phased array systems. Such a possibility could open new paths in the way light sources are incorporated and utilized in small scales.

Work at FORTH was supported by Greek GSRT Project ERC02-EXEL Grant No. 6260 and by the European Research Council under the ERC Advanced Grant No. 320081 (PHOTOMETA). The work at Ames Laboratory was partially supported by the U.S. Department of Energy (Basic Energy Science, Division of Materials Sciences and Engineering) under Contract No. DE-AC02-07CH11358 and by the U.S. Office of Naval Research, Grant No. N00014-14-1-0474.

- *sdroulias@iesl.forth.gr
- [1] K. Iga, *IEEE J. Sel. Top. Quantum Electron.* **6**, 1201 (2000).
- [2] O. Painter, R. K. Lee, A. Scherer, A. Yariv, J. D. O'Brien, P. D. Dapkus, and I. Kim, *Science* **284**, 1819 (1999).
- [3] A. Tandaechanurat, S. Ishida, D. Guimard, M. Nomura, S. Iwamoto, and Y. Arakawa, *Nat. Photonics* **5**, 91 (2011).
- [4] S. L. McCall, A. F. J. Levi, R. E. Slusher, S. J. Pearton, and R. A. Logan, *Appl. Phys. Lett.* **60**, 289 (1992).
- [5] J. P. Zhang, D. Y. Chu, S. L. Wu, S. T. Ho, W. G. Bi, C. W. Tu, and R. C. Tiberio, *Phys. Rev. Lett.* **75**, 2678 (1995).
- [6] D. J. Bergman and M. I. Stockman, *Phys. Rev. Lett.* **90**, 027402 (2003).
- [7] M. I. Stockman, *Nat. Photonics* **2**, 327 (2008).
- [8] N. I. Zheludev, S. L. Prosvirmin, N. Papisimakis, and V. A. Fedotov, *Nat. Photonics* **2**, 351 (2008).
- [9] R. F. Oulton, V. J. Sorger, T. Zentgraf, R.-M. Ma, C. Gladden, L. Dai, G. Bartal, and X. Zhang, *Nature (London)* **461**, 629 (2009).
- [10] M. A. Noginov, G. Zhu, A. M. Belgrave, R. Bakker, V. M. Shalaev, E. E. Narimanov, S. Stout, E. Herz, T. Suteewong, and U. Wiesner, *Nature (London)* **460**, 1110 (2009).
- [11] P. Berini and I. De Leon, *Nat. Photonics* **6**, 16 (2012).
- [12] S. Wuestner, A. Pusch, K. L. Tsakmakidis, J. M. Hamm, and O. Hess, *Phys. Rev. Lett.* **105**, 127401 (2010).
- [13] O. Hess, J. B. Pendry, S. A. Maier, R. F. Oulton, J. M. Hamm, and K. L. Tsakmakidis, *Nat. Mater.* **11**, 573 (2012).
- [14] X. L. Zhong and Z. Y. Li, *Phys. Rev. B* **88**, 085101 (2013).
- [15] A. Jain, P. Tassin, T. Koschny, and C. M. Soukoulis, *Phys. Rev. Lett.* **112**, 117403 (2014).
- [16] N. Meinzer, M. Ruther, S. Linden, C. M. Soukoulis, G. Khitrova, J. Hendrickson, J. D. Olitzky, H. M. Gibbs, and M. Wegener, *Opt. Express* **18**, 24140 (2010).
- [17] N. Meinzer, M. König, M. Ruther, S. Linden, G. Khitrova, H. M. Gibbs, K. Busch, and M. Wegener, *Appl. Phys. Lett.* **99**, 111104 (2011).
- [18] A. Fang, T. Koschny, and C. M. Soukoulis, *J. Opt.* **12**, 024013 (2010).
- [19] Z. Huang, T. Koschny, and C. M. Soukoulis, *Phys. Rev. Lett.* **108**, 187402 (2012).
- [20] Z. Huang, S. Droulias, T. Koschny, and C. M. Soukoulis, *Opt. Express* **22**, 28596 (2014).
- [21] A. Taflove, *Computational Electrodynamics: The Finite Difference Time Domain Method* (Artech House, London, 1995).
- [22] A. E. Siegman, *Lasers* (University Science, Sausalito, CA, 1986).
- [23] See Supplemental Material at <http://link.aps.org/supplemental/10.1103/PhysRevLett.118.073901> for the methods and for additional numerical results.
- [24] The pumping rate is equivalent to a pump intensity. The pump power density is equal to $\hbar\omega_a R_p N_0$, and the pump intensity $I_p = (\text{pump power})/(\text{surface area}) = \hbar\omega_a R_p N_0 (\text{volume})/(\text{surface area}) = \hbar\omega_a R_p N_0 d$, and d is the thickness of the gain layer. If we use the numbers of our simulations, $R_p = 4.4 \times 10^6 \text{ s}^{-1}$, $N_0 = 5 \times 10^{23} \text{ m}^{-3}$, $\omega_a = 2\pi \times 196 \text{ THz}$, and $d = 60 \text{ nm}$, then $I_p = 0.017 \text{ W/mm}^2$.
- [25] The equivalent boundary conditions for the current sheet are $\mathbf{n} \times (\mathbf{E}_2 - \mathbf{E}_1) = -\mathbf{j}_m$, $\mathbf{n} \times (\mathbf{H}_2 - \mathbf{H}_1) = \mathbf{j}_e$, where \mathbf{n} is the surface normal of the current sheet pointing from region 1 to region 2. In the actual system, the dark mode oscillates along the z axis and produces z -polarized waves; hence, in the equivalent sheet model it is assumed that $\mathbf{j}_e = j_e \mathbf{z}$ and $\mathbf{j}_m = j_m \mathbf{x}$. Consequently, the outgoing electric and magnetic fields are expressed as $\mathbf{E}^\pm = E_z^\pm \mathbf{z} = -\frac{1}{2}(\eta j_e \pm j_m) e^{i(\omega t \mp ky)} \mathbf{z}$ and $\mathbf{H}^\pm = H_x^\pm \mathbf{x} = \pm(1/\eta) E_z^\pm \mathbf{x}$ respectively, where η is the vacuum impedance and the sign corresponds to the respective direction of emission along the y axis. The time-averaged Poynting vector along each side of the current sheet is then expressed via the equivalent currents as $\langle \mathbf{S} \rangle^\pm = \frac{1}{2} \text{Re}(\mathbf{E}^\pm \times \mathbf{H}^{\pm*})$, where the asterisk denotes the complex conjugate.